Parallel Computing Based Solution for Reliability-constrained Distribution Network Planning

Yaqi Sun, Wenchuan Wu, *Fellow*, *IEEE*, Yi Lin, Hai Huang, and Hao Chen

***Abstract*—The main goal of distribution network (DN) expansion planning is essentially to achieve minimal investment constrained by specified reliability requirements. The reliability-constrained distribution network planning (RcDNP) problem can be cast as an instance of mixed-integer linear programming (MILP) which involves ultra-heavy computation burden especially for large-scale DNs. In this paper, we propose a parallel computing based solution method for the RcDNP problem. The RcDNP is decomposed into a backbone grid and several lateral grid problems with coordination. Then, a parallelizable augmented Lagrangian algorithm with acceleration method is developed to solve the coordination planning problems. The lateral grid problems are solved in parallel through coordinating with the backbone grid planning problem. Gauss-Seidel iteration is adopted on the subset of the convex hull of the feasible region constructed by decomposition. Under mild conditions, the optimality and convergence of the proposed method are proven. Numerical tests show that the proposed method can significantly reduce the solution time and make the RcDNP applicable for real-world problems.**

***Index Terms*—Distribution network, expansion planning, reliability, parallel computing.**

NOMENCLATURE

A. Sets and Vectors

Λ_C Set of alternative types of conductors

Λ_T Set of alternative types of transformers

Ψ_B Set of branches

Ψ_F Set of feeders

Ψ_N Set of nodes

Ψ_{SS} Set of substation nodes

Ψ_T Set of transformers

Ψ_{Tr}^{out} Set of transformer outlet branches

Ψ_i Set of nodes connected to node i

Ψ_D^e Set of equivalent load nodes in backbone grid

Ψ_S^e Set of equivalent source nodes in sub-area

$D_b, D_{s,n}$ Subsets of convex hull $conv(X_b)$ and $conv(X_{s,n})$

$\boldsymbol{e}_t$ Unit vector whose elements are equal to 0 except the t^{th} element that is equal to 1

$\boldsymbol{g}_C^{a,\tau}, \boldsymbol{g}_C^{a,0}, \boldsymbol{g}_T^{a,\tau}, \boldsymbol{g}_T^{a,0}$ Aging vectors for conductors and transformers

$\boldsymbol{w}_b, \boldsymbol{w}_{s,n}$ Vectors of Lagrangian multipliers

$\boldsymbol{x}_b, \boldsymbol{x}_{s,n}$ Vectors of decision variables of backbone grid and the n^{th} sub-area planning model

$X_b, X_{s,n}$ Feasible sets of backbone grid and the n^{th} sub-area planning model

X_i Feasible set

$\boldsymbol{x}_i, \boldsymbol{z}_i$ Vectors of decision variables and coordination variables

$\boldsymbol{z}_b, \boldsymbol{z}_{s,n}$ Vectors of coordination variables describing boundary conditions for backbone grid and the n^{th} sub-area planning model

$(\cdot)^k$ Variables in the k^{th} iteration

B. Parameters

$\tau_{xy}^{SW}, \tau_{xy}^{RP}$ Durations of switching-only interruptions and repair-and-switching interruptions associated with failure of branch connecting nodes x and y

ω Cost coefficient of energy not supplied

$\tau(t)$ Number of year up to stage t

δ_t^I Present value factor for investment costs at stage t

δ_t^O Present value factor for maintenance costs at stage t

ε_{SAIDI}^t System average interruption duration index (SAIDI) requirement at stage t

ρ Penalty value

$C_C^{a,I}$ Investment cost for alternative conductor a

$C_C^{a,M}$ Maintenance cost for alternative conductor a

$C_T^{a,I}$ Investment cost for alternative transformer a

Manuscript received: October 6, 2023; revised: December 26, 2023; accepted: January 5, 2024. Date of CrossCheck: January 5, 2024. Date of online publication: March 20, 2024.

This work was supported in part by the State Grid Science and Technology Program of China (No. 5100-202121561A-0-5-SF).

Y. Sun and W. Wu (corresponding author) are with the State Key Laboratory of Power Systems, Department of Electrical Engineering, Tsinghua University, Beijing 100084, China, and they are also with Sichuan Energy Internet Research Institute, Tsinghua University, Chengdu, China (e-mail: sun-yq20@mails.tsinghua.edu.cn; wuwench@tsinghua.edu.cn).

Y. Lin, H. Huang, and H. Chen are with State Grid Fujian Electric Power Co. Ltd., Fuzhou, China (e-mail: liny-02@qq.com; huang_hai@fj.sgcc.com.cn; haochen_zju@163.com).

DOI: 10.35833/MPCE.2023.000760

$C_T^{a,M}$ Maintenance cost for alternative transformer a

$C_S^{s,I}$ Investment cost for substation at node s

$C_S^{s,M}$ Maintenance cost for substation at node s

d_{ij} Distance between node i and node j

$l_{ij}^{a,0}$ Parameter equal to 1 when type a conductor exists at branch ij originally

$m_{Tr}^{a,0}$ Parameter equal to 1 when type a transformer exists at transformer Tr originally

M A sufficiently large positive constant

N_s The maximum number of transformers in substation

n Number of subproblems

n_s^0 Parameter equal to 1 when a substation exists at node s originally

n_{sub} Number of sub-areas

NC_i^t Number of customers at node i at stage t

r_C^a Resistance unit of type a conductor

S_C^a Capacity of type a conductor

S_T^a Capacity of type a transformer

x_C^a Inductance unit of type a conductor

$\underline{(\cdot)}, \overline{(\cdot)}$ Lower and upper bounds of variable $(\cdot)$

C. Continuous Variables

λ_{ij}^t Failure rate of branch ij at stage t

τ_{ij}^t Repair time of branch ij at stage t

CIF_i^t Customer interruption frequency (CIF) of node i at stage t

CID_i^t Customer interruption duration (CID) of node i at stage t

$CIF_i^{e,t}$ Temporarily estimated CIF of equivalent load node (ELN) i at stage t

$CID_i^{e,t}$ Temporarily estimated CID of ELN i at stage t

$EENS^t$ Expected energy not supplied at stage t

$h_i^{f,t}$ Variable in the range of [0, 1] and equal to 1 when node i is supplied by feeder f under normal operation condition at stage t

$h_{ij}^{f,t}$ Variable in the range of [0, 1] and equal to 1 when branch ij is supplied by feeder f under normal operation condition at stage t

$n_i^{xy,t}$ Substitution variable of product term $\lambda_{xy}^t \tau_{xy}^t p_i^{xy,t}$ for equivalent outlet branch of equivalent distribution source in sub-area at stage t

r_{ij}^t Resistance of branch ij at stage t

P_i^t, Q_i^t Active and reactive load demands of node i at stage t

$P_i^{d,t}, Q_i^{d,t}$ Equivalent active and reactive loads of sub-area at node i at stage t

$P_i^{xy,t}$, $Q_i^{xy,t}$ Active and reactive demands at node i after post-fault network reconfiguration due to a fault at branch xy (xy=NO represents normal operation condition) at stage t

$P_{i,g}^{xy,t}$, $Q_{i,g}^{xy,t}$ Active and reactive outputs of distributed generation at node i after post-fault network reconfiguration due to a fault in branch xy (xy=NO represents normal operation condition) at stage t

$P_{ij}^{xy,t}$, $Q_{ij}^{xy,t}$ Active and reactive power flows through branch ij (from node i to node j) after post-fault network reconfiguration due to a fault in branch xy (xy=NO represents normal operation condition) at stage t

$P_{Tr}^{xy,t}$, $Q_{Tr}^{xy,t}$ Active and reactive power flows through transformer Tr after post-fault network reconfiguration due to a fault at branch xy (xy=NO represents normal operation condition) at stage t

$S_{ij}^{C,t}$ Capacity of branch ij at stage t

$S_{Tr}^{C,t}$ Capacity of transformer Tr at stage t

$SAIDI^t$ SAIDI at stage t

u_{xy}^t Substitution variable for product of failure rate λ_{xy}^t and repair time τ_{xy}^t of equivalent outlet branch (EOB) xy at stage t

$U_i^{ss,t}$ Square of voltage at reference node i at stage t

$U_i^{xy,t}$ Square of voltage at node i due to a fault at branch xy (xy=NO represents normal operation condition) at stage t

x_{ij}^t Inductance of branch ij at stage t

D. Binary Variables

l_{ij}^t Binary variable equal to 1 when there exists a conductor at branch ij, otherwise equal to 0 at stage t

$l_{ij}^{a,t}$ Binary variable equal to 1 when alternative conductor a at branch ij is installed, otherwise equal to 0 at stage t

m_{Tr}^t Binary variable equal to 1 when transformer Tr exists, otherwise equal to 0 at stage t

$m_{Tr}^{a,t}$ Binary variable equal to 1 when alternative transformer a at candidate position Tr is installed, otherwise equal to 0 at stage t

n_s^t Binary variable equal to 1 when substation at node s is built, otherwise equal to 0 at stage t

$p_i^{xy,t}$ Binary variable equal to 1 when node i is affected by outage due to a fault in branch xy at stage t

$q_i^{xy,t}$ Binary variable equal to 1 when node i is still in outage after network reconfiguration following a fault in branch xy at stage t

$s_{ij}^{xy,t}$ Binary variable equal to 1 when branch ij is connected after network reconfiguration due to a fault in branch xy (xy=NO represents normal operation condition) at stage t

I. Introduction

In order to improve the reliability of power supply, mesh-designed architecture is commonly adopted in the current urban distribution networks (DNs). The DN operates radially under normal conditions, and redundant lines are used for power rerouting after failures [1]-[3]. Therefore, the DN with mesh structure has higher reliability [4]. When calculating the reliability index of the mesh-designed DN, it is necessary to consider the fault isolation and load transfer after the fault, which can be achieved through network reconfiguration. Otherwise, the reliability of the DN may be underestimated [5]. Since different customers or lateral grids have different power supply reliability criteria, the DN expansion planning scheme is optimized to achieve the minimum investment cost constrained by specified reliability requirements. Commonly used reliability indicators include customer interruption frequency (CIF), customer interruption duration (CID), system average interruption frequency index (SAIFI), and system average interruption duration index (SAIDI) [6], [7].

DN planning considering reliability has been studied. However, early researches mostly penalize the expectation of power loss in the objective function, which implicitly and approximately reflects the reliability of DNs [8], [9]. With the improvement of relevant standards, some quantitative indices are used to measure the reliability of DNs [7], [10]. In order to make the planning results meet the specified reliability requirements, the reliability assessment process is required during optimization, which can be achieved by simulation-based methods or analytical methods.

Simulation-based methods often use iterative optimization assessment procedure, i.e., optimization steps are performed with a posterior reliability assessment program [11]-[15]. In [11], a pool of feasible solutions with diverse expansion plans is first obtained, and the reliability index of each plan is calculated to determine the optimal solution. A comprehensive planning methodology is proposed in [12] considering upgrading the conventional equipment in the DNs. The entire solution process includes the optimal DN reinforcement and the power flow solution process based on Gauss-Seidel iteration, which is used to evaluate the performance of the reinforcement scheme. Based on [11], the choices of customers on reliability have been considered in DN planning model by carrying out Monte Carlo based simulation in the solution process [13]. An integrated method for reliability planning and risk estimation in DNs is proposed in [14], which takes the backup supply or automatic/manual reconfiguration schemes into the consideration. The reliability assessment part of [14] still relies on the time-sequential Monte Carlo based simulation. Decision tree is used in [15] to solve multi-stage network planning problem, in which the switchgear optimization is implemented by simulation software. Tabu search is adopted in [16] to solve the DN planning model considering uncertainty, which requires evaluations to determine the movements for the next search step. Genetic algorithm involving reliability assessment procedure to calculate the fitness function is used for reliability planning stage in [17]. The simulation-based method is intuitive and easy to implement, but suffers from long solution time. The evaluation procedure cannot be embedded in the planning model to obtain a joint solution, while the iterative heuristic method cannot guarantee optimality.

Meanwhile, the analytical solution method of the reliability index has been studied in some literatures. Based on the analytical solution model of reliability, some pioneer works have embedded analytical reliability constraints into the DN planning model. Based on the fault incidence matrix proposed in [18], the fault incidence matrix is applied in [19] for the joint optimization configuration of sectional switches and tie-lines. Linearized models of different reliability indices are introduced in [20] and then involved in a mixed-integer linear programming (MILP) model of DN planning. Network modeling formulation of reliability indices are derived in [21] and [22] to consider events such as fault isolation and load restoration in DN planning. The multi-level expansion planning problem of the DN is modeled in [23] as an MILP, which has good convergence and can be solved efficiently. However, the post-fault load restoration which can improve the reliability of DNs [5] is not fully considered. For mesh DNs, planning schemes without tie switches for post-fault load restoration may lead to excessive investment.

Post-fault load restoration is considered in the DN planning model proposed in [24], but the model is solved by heuristic algorithm. Inspired by [23], a reliability-constrained DN planning (RcDNP) considering post-fault load restoration for mesh DNs is proposed in [25]. The DN expansion planning problem is finally formulated as an MILP. However, the model proposed in [25] does not take the sparse nature of the topological connection relationship of the DN into consideration. Existing studies usually model RcDNP as MILP. As the scale of the DN expands, the number of decision variables in the centralized planning model will explosively grow, making it challenging to handle due to the escalating model complexity. Furthermore, with the proliferation of decision variables, the search space of the MILP problem also expands significantly, leading to reduced solution efficiency. This makes it challenging to find the optimal solution or even a feasible solution within an acceptable timeframe. Planners often need to change the boundary conditions of the problem to create different planning scenarios, rather than forming a single plan at once. This requires repetitive calculations, making the centralized model unsuitable for practical applications.

As an effective mean to improve solution efficiency, parallel computing has been widely applied in power system optimization such as distributed optimal power flow [26] and distributed reactive power control [27]. However, distributed optimization algorithms adopted in the existing literature such as alternating direction method of multipliers (ADMM) [28] and analytical target cascading (ATC) [29] cannot be used directly in solving the RcDNP problem, since it is an MILP involving a large number of integer variables. A parallel computing method combining branch exchange and dynamic programming for large-scale network layout optimization has been proposed in [30]. Based on [30], the simultaneous optimization of the line layout and type of conductor is further implemented in [31]. But the branch exchange algorithm adopted in network structure optimization still relies on heuristic search and is only suitable for radial DNs. In [32], a genetic algorithm based planning method is proposed considering the sparseness of the rural DN. Reference [33] has established an MILP model for radial DN expansion planning. This model decomposes the original planning problem into several sub-problems and employs a simulated annealing algorithm for the iterative solution. In [34], the load points of the DN are decomposed into different substation supply areas, and subsequently, the static substation planning problem is addressed using an evolutionary algorithm. A parallelizable solution method based on the genetic algorithm is introduced in [35], wherein the genetic algorithm is initially employed for solving the sub-problems in parallel. Subsequently, the fitness function of the integrated solution is decomposed to update the solutions of the sub-problems. Reference [36] divides the planning region into smaller sub-regions during the DN planning process. These smaller sub-regions are independently optimized using heuristic methods. Based on the optimization at the sub-regional level, a global analysis of the planning region is then conducted. However, the heuristic method is not stable and the optimality of the solution cannot be guaranteed theoretically. Parallel accelerated solution method for large-scale mesh DN expansion planning remains to be further studied.

Built upon [25], this paper presents a parallel computing based solution method for RcDNP to overcome the above difficulties. Firstly, the RcDNP model is reformulated to the backbone grid and sub-areas. Then, a parallelizable augmented Lagrangian algorithm is adopted to solve the model in parallel manner. Furthermore, the Nesterov acceleration method with restart is used to improve the convergence speed.

The main contributions of this paper are summarized as follows.

1) A decomposed RcDNP model is proposed, in which the planning grid is decomposed into the backbone grid and several sub-areas. The number of integer variables of the planning problem roughly increases linearly with the size of the planning DN, while the centralized RcDNP model in [25] increases quadratically.

2) A parallelizable augmented Lagrangian algorithm with acceleration method is developed to solve the coordination planning problem involving the backbone grid and sub-areas. Numerical tests show that the proposed parallel computing based solution method exhibits a linearly increasing computation time with the growing size of DNs. The optimality and convergence of the algorithm is also proved rigorously.

The remainder of this paper is arranged as follows. The mathematical formulation of the RcDNP model for the backbone grid and sub-area is introduced in Section II. The parallel solution process with acceleration method is discussed in Section III. Numerical tests and results are demonstrated to illustrate the performance of the proposed solution method in Section IV. Conclusions are drawn in Section V.

II. Mathematical Formulation of RcDNP Model

A. Decomposed Planning Model

In the DN, substations are designed to supply power to multiple load concentrated areas. These load concentrated areas are connected to the substation through the backbone grid. This natural sparse structure inspires us to decompose the RcDNP problem into the backbone grid and sub-area planning problems. It can be solved in parallel through coordination. The decomposed planning model is shown in Fig. 1.

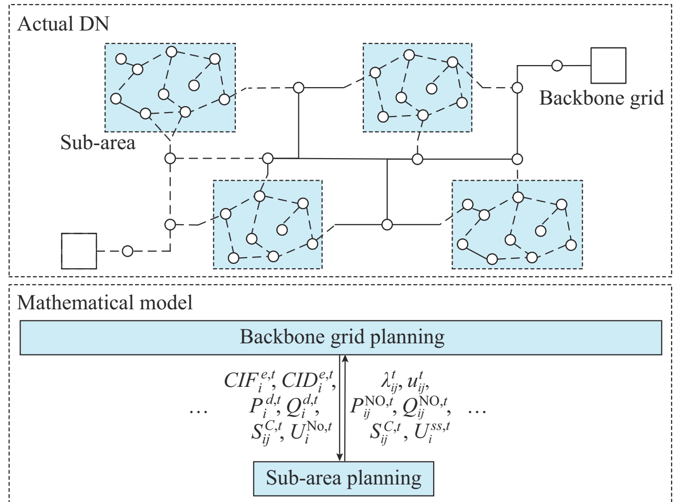

Fig. 1. Decomposed planning model.

The proposed model consists of three parts: backbone grid planning module, sub-area planning module, and coordination layer. As shown in Fig. 2, the sub-area is aggregated as an equivalent load node (ELN) i' in the backbone grid planning. For the sub-area planning, the backbone grid is represented by an equivalent distribution source (EDS) i'' connected a series equivalent outlet branch (EOB) $i''j''$ with a certain probability of failure.

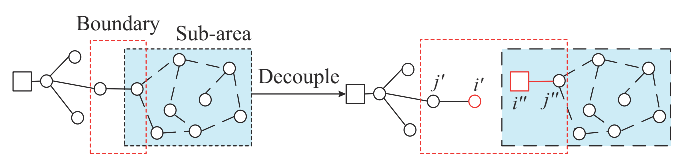

Fig. 2. Schematic diagram of equivalent decoupled models of backbone grid and sub-area for RcDNP.

The consistency conditions of boundary variables include two aspects: the consistency of the power flow and the consistency of the reliability index.

The consistency of the power flow means that the equivalent load of the backbone grid should be equal to the power flow of corresponding EOB in the sub-area. Besides, corresponding branches in the backbone grid and sub-area share the same capacity while corresponding nodes in the backbone grid and sub-area share the same voltage.

$$P_{i'}^{d,t}=P_{i''j''}^{\mathrm{NO},t} \quad i'\in \Psi_D^e, i''\in \Psi_S^e, j''\in \Psi_{i''} \tag{1}$$

$$Q_{i'}^{d,t}=Q_{i''j''}^{\mathrm{NO},t} \quad i'\in \Psi_D^e, i''\in \Psi_S^e, j''\in \Psi_{i''} \tag{2}$$

$$S_{i'j'}^{C,t}=S_{i''j''}^{C,t} \quad i'\in \Psi_D^e, i''\in \Psi_S^e, j'\in \Psi_{i'}, j''\in \Psi_{i''} \tag{3}$$

$$U_{i'}^{\mathrm{NO},t}=U_{i''}^{ss,t} \quad i'\in \Psi_D^e, i''\in \Psi_S^e \tag{4}$$

The consistency of the reliability index means that the parameter of the EOB in the sub-area and the reliability index of the ELN of the backbone grid should meet the following constraints.

$$\lambda_{i''j''}^{t}=CIF_{i'}^{e,t} \quad i'\in \Psi_D^e, i''\in \Psi_S^e, j''\in \Psi_{i''} \tag{5}$$

$$\tau_{i''j''}^{t}=CID_{i'}^{e,t}/CIF_{i'}^{e,t} \quad i'\in \Psi_D^e, i''\in \Psi_S^e, j''\in \Psi_{i''} \tag{6}$$

The EDS i'' is assumed to be completely reliable, and the influence of the backbone grid failures on the sub-area is reflected in the EOB.

B. Objective Function

The objective function for the RcDNP model is the total investment, which consists of investment cost, maintenance cost, and reliability cost.

$$\min f(\boldsymbol{x})=\sum_{t=1}^{T}[\delta_t^I c_t^I+\delta_t^O(c_t^M+\omega\cdot EENS^t)] \tag{7}$$

The investment cost c_t^I and the maintenance cost c_t^M at stage t are defined as:

$$c_t^I=\sum_{ij\in\Psi_B}\sum_{a\in\Lambda_C}C_C^{a,I}l_{ij}^{a,t}+\sum_{Tr\in\Psi_T}\sum_{a\in\Lambda_T}C_T^{a,I}m_{Tr}^{a,t}+\sum_{s\in\Psi_{SS}}C_S^{s,I}n_s^t \tag{8}$$

$$\begin{aligned}c_t^M=&\boldsymbol{e}_t^{\mathrm{T}}\sum_{ij\in\Psi_B}\sum_{a\in\Lambda_C}C_C^{a,M}\left(\sum_{\tau=1}^{t}l_{ij}^{a,\tau}\boldsymbol{g}_C^{a,\tau}+l_{ij}^{a,0}\boldsymbol{g}_C^{a,0}\right)+\\&\boldsymbol{e}_t^{\mathrm{T}}\sum_{Tr\in\Psi_T}\sum_{a\in\Lambda_T}C_T^{a,M}\left(\sum_{\tau=1}^{t}m_{Tr}^{a,t}\boldsymbol{g}_T^{a,\tau}+m_{Tr}^{a,0}\boldsymbol{g}_T^{a,0}\right)+\\&\sum_{s\in\Psi_{SS}}C_S^{s,M}\left(\sum_{t=1}^{t}n_s^t+n_s^0\right)\end{aligned} \tag{9}$$

C. Constraints

The constraints in the model include the following.

1) Operation Constraints

Operation constraints are classified into normal conditions and fault conditions.

$$-M(1-s_{ij}^{xy,t})\le U_j^{xy,t}-U_i^{xy,t}+2(r_{ij}^tP_{ij}^{xy,t}+x_{ij}^tQ_{ij}^{xy,t}) \quad \forall ij\in\Psi_B \tag{10}$$

$$U_j^{xy,t}-U_i^{xy,t}+2(r_{ij}^tP_{ij}^{xy,t}+x_{ij}^tQ_{ij}^{xy,t})\le M(1-s_{ij}^{xy,t}) \quad \forall ij\in\Psi_B \tag{11}$$

$$\sum_{j\in\Psi_i}P_{ij}^{xy,t}+P_i^{xy,t}+P_{i,g}^{xy,t}=0 \quad \forall i\in\Psi_N \tag{12}$$

$$\sum_{j\in\Psi_i}Q_{ij}^{xy,t}+Q_i^{xy,t}+Q_{i,g}^{xy,t}=0 \quad \forall i\in\Psi_N \tag{13}$$

$$\underline{U}\le U_i^{xy,t}\le\overline{U} \quad \forall i\in\Psi_N \tag{14}$$

$$U_i^{xy,t}=U_i^{ss,t} \quad \forall i\in\Psi_{SS} \tag{15}$$

$$\begin{cases}P_{Tr}^{xy,t}=P_{ij}^{xy,t}\\Q_{Tr}^{xy,t}=Q_{ij}^{xy,t}\end{cases} \quad Tr\in\Psi_T, ij\in\Psi_{Tr}^{out} \tag{16}$$

$$\begin{cases}-Ms_{ij}^{xy,t}\le P_{ij}^{xy,t}\le Ms_{ij}^{xy,t}\\-S_{ij}^{C,t}\le P_{ij}^{xy,t}\le S_{ij}^{C,t}\\-Ms_{ij}^{xy,t}\le Q_{ij}^{xy,t}\le Ms_{ij}^{xy,t}\\-S_{ij}^{C,t}\le Q_{ij}^{xy,t}\le S_{ij}^{C,t}\end{cases} \quad \forall ij\in\Psi_B \tag{17}$$

$$-\sqrt{2}\,S_{ij}^{C,t}\le P_{ij}^{xy,t}\pm Q_{ij}^{xy,t}\le\sqrt{2}\,S_{ij}^{C,t} \quad \forall ij\in\Psi_B \tag{18}$$

$$\begin{cases}P_{Tr}^{xy,t}\le S_{Tr}^{C,t}\\Q_{Tr}^{xy,t}\le S_{Tr}^{C,t}\end{cases} \quad \forall Tr\in\Psi_T \tag{19}$$

$$-\sqrt{2}\,S_{Tr}^{C,t}\le P_{Tr}^{xy,t}\pm Q_{Tr}^{xy,t}\le\sqrt{2}\,S_{Tr}^{C,t} \quad \forall Tr\in\Psi_T \tag{20}$$

$$s_{ij}^{xy,t}\le l_{ij}^t \quad \forall ij\in\Psi_B \tag{21}$$

Here $xy\in\Psi_B\bigcup\{\mathrm{NO}\}$ represents the branch fault set and normal operation. The linearized power flow constraints, power balance constraints, voltage constraints, and capacity constraints are given in (10)-(20). Constraint (21) indicates that the connecting status is equal to zero when there is no branch constructed.

2) Fault Indicator Variable Constraints

$$s_{xy}^{xy,t}=0 \tag{22}$$

$$h_i^{f,t}+h_{xy}^{f,t}-1\le p_i^{xy,t} \quad \forall f\in\Psi_F, \forall i\in\Psi_N \tag{23}$$

$$p_i^{xy,t}\ge q_i^{xy,t} \quad \forall i\in\Psi_N \tag{24}$$

$$\begin{cases}P_i^{xy,t}=P_i^t(1-q_i^{xy,t})\\Q_i^{xy,t}=Q_i^t(1-q_i^{xy,t})\end{cases} \quad \forall i\in\Psi_N \tag{25}$$

$$\sum_{ij}s_{ij}^{xy,t}=\sum_{i}(1-q_i^{xy,t}) \quad ij\in\Psi_B, i\in\Psi_N, i\notin\Psi_{SS} \tag{26}$$

$$-M(1-s_{ij}^{\mathrm{NO},t})+h_i^{f,t}\le h_{ij}^{f,t}\le h_i^{f,t}+M(1-s_{ij}^{\mathrm{NO},t}) \quad \forall ij\in\Psi_B, \forall f\in\Psi_F \tag{27}$$

$$-M(1-s_{ij}^{\mathrm{NO},t})+h_j^{f,t}\le h_{ij}^{f,t}\le h_j^{f,t}+M(1-s_{ij}^{\mathrm{NO},t}) \quad \forall ij\in\Psi_B, \forall f\in\Psi_F \tag{28}$$

$$h_{ij}^{f,t}=s_{ij}^{\mathrm{NO},t} \quad \text{if line } ij \text{ is outlet branch of feeder } f \tag{29}$$

$$h_{ij}^{f,t}\le s_{ij}^{\mathrm{NO},t} \quad \forall ij\in\Psi_B, \forall f\in\Psi_F \tag{30}$$

$$\sum_f h_i^{f,t}\le 1 \quad \forall i\in\Psi_N \tag{31}$$

$$\sum_f h_{ij}^{f,t}\le 1 \quad \forall ij\in\Psi_B \tag{32}$$

$$\sum_{ij}s_{ij}^{\mathrm{NO},t}=\sum_f\sum_i h_i^{f,t} \quad ij\in\Psi_B, f\in\Psi_F, i\in\Psi_N, i\notin\Psi_{SS} \tag{33}$$

Here $xy\in\Psi_B$ represents the failure scenario. Constraint (22) indicates that branch xy is outage and isolated in the scenario where branch xy fails. Constraint (23) determines that the affected nodes by the outage of branch xy must share the same feeder affiliation variable with the one of branch xy. Constraint (24) indicates the nodes not affected by the fault cannot loss power supply due to network reconfiguration. Constraint (25) indicates that if the node can restore power supply after the post-fault network reconfiguration, its load level returns to the normal state; otherwise, it remains in the outage state. Constraints (27)-(30) are for the feeder affiliation variables related to the network topology in normal state, where (27) and (28) show that feeder affiliation variables can be propagated if branch ij is connected under normal operation conditions. Constraints (26) and (31)-(33) are radial operation constraints under normal and fault conditions [25].

Regarding the problem of backbone grid planning, the following constraints need to be attached.

$$P_i^t=\begin{cases}P_i^{\mathrm{NO},t} & \forall i\in\Psi_N, i\notin\Psi_D^e\\ P_i^{d,t} & \forall i\in\Psi_N, i\in\Psi_D^e\end{cases} \tag{34}$$

$$Q_i^t=\begin{cases}Q_i^{\mathrm{NO},t} & \forall i\in\Psi_N, i\notin\Psi_D^e\\ Q_i^{d,t} & \forall i\in\Psi_N, i\in\Psi_D^e\end{cases} \tag{35}$$

3) Equipment Selection Constraints

$$l_{ij}^t=\boldsymbol{e}_t^{\mathrm{T}}\sum_{a\in\Lambda^C}\left(\sum_{\tau=1}^{t}l_{ij}^{a,\tau}\boldsymbol{g}_C^{a,\tau}+l_{ij}^{a,0}\boldsymbol{g}_C^{a,0}\right)\quad\forall ij\in\Psi_B \tag{36}$$

$$S_{ij}^{C,t}=\boldsymbol{e}_t^{\mathrm{T}}\sum_{a\in\Lambda^C}S_C^a\left(\sum_{\tau=1}^{t}l_{ij}^{a,\tau}\boldsymbol{g}_C^{a,\tau}+l_{ij}^{a,0}\boldsymbol{g}_C^{a,0}\right)\quad\forall ij\in\Psi_B \tag{37}$$

$$r_{ij}^t=d_{ij}\boldsymbol{e}_t^{\mathrm{T}}\sum_{a\in\Lambda^C}r_C^a\left(\sum_{\tau=1}^{t}l_{ij}^{a,\tau}\boldsymbol{g}_C^{a,\tau}+l_{ij}^{a,0}\boldsymbol{g}_C^{a,0}\right)\quad\forall ij\in\Psi_B \tag{38}$$

$$x_{ij}^t=d_{ij}\boldsymbol{e}_t^{\mathrm{T}}\sum_{a\in\Lambda^C}x_C^a\left(\sum_{\tau=1}^{t}l_{ij}^{a,\tau}\boldsymbol{g}_C^{a,\tau}+l_{ij}^{a,0}\boldsymbol{g}_C^{a,0}\right)\quad\forall ij\in\Psi_B \tag{39}$$

$$\lambda_{ij}^t=d_{ij}\boldsymbol{e}_t^{\mathrm{T}}\sum_{a\in\Lambda^C}\lambda_C^a\left(\sum_{\tau=1}^{t}l_{ij}^{a,\tau}\boldsymbol{g}_C^{a,\tau}+l_{ij}^{a,0}\boldsymbol{g}_C^{a,0}\right)\quad\forall ij\in\Psi_B \tag{40}$$

$$m_{Tr}^t=\boldsymbol{e}_t^{\mathrm{T}}\sum_{a\in\Lambda^T}\left(\sum_{\tau=1}^{t}m_{Tr}^{a,\tau}\boldsymbol{g}_T^{a,\tau}+m_{Tr}^{a,0}\boldsymbol{g}_T^{a,0}\right)\quad\forall Tr\in\Psi_T \tag{41}$$

$$S_{Tr}^{C,t}=\boldsymbol{e}_t^{\mathrm{T}}\sum_{a\in\Lambda^T}S_{Tr}^a\left(\sum_{\tau=1}^{t}m_{Tr}^{a,\tau}\boldsymbol{g}_T^{a,\tau}+m_{Tr}^{a,0}\boldsymbol{g}_T^{a,0}\right)\quad\forall Tr\in\Psi_T \tag{42}$$

$$\sum_{\tau=1}^{t}n_s^\tau+n_s^0\le 1\quad\forall s\in\Psi_{SS} \tag{43}$$

$$\sum_{\tau=1}^{t}\sum_{Tr\in\Psi_T}m_{Tr}^\tau\le N_s\left(\sum_{\tau=1}^{t}n_s^\tau+n_s^0\right)\quad\forall s\in\Psi_{SS} \tag{44}$$

Constraints (36)-(43) indicate that an available equipment must already exist or be constructed at the planning stage. Logic constraint between the installation of transformers and the existence of substation is demonstrated as constraint (44).

4) Calculation of Reliability Index

$$CID_i^t=\sum_{xy\in\Psi_B}\lambda_{xy}^t\tau_{xy}^{SW}p_i^{xy,t}+\sum_{xy\in\Psi_B}\lambda_{xy}^t(\tau_{xy}^{RP}-\tau_{xy}^{SW})q_i^{xy,t}\quad\forall i\in\Psi_N \tag{45}$$

$$SAIDI^t=\sum_{i\in\Psi_N}NC_i^t\cdot CID_i^t\Big/\sum_{i\in\Psi_N}NC_i^t \tag{46}$$

$$SAIDI^t\le\varepsilon_{SAIDI}^t \tag{47}$$

Equations (45) and (46) are the commonly used reliability indices, and (47) is the reliability constraint expressed by SAIDI. For the sub-area planning problem, since the failure rate and repair time of the EOB are also variables, (45) should be rewritten as:

$$CID_i^t=\sum_{\substack{x\notin\Psi_S^e\\ y\in\Psi_x}}\lambda_{xy}^t\tau_{xy}^{SW}p_i^{xy,t}+\sum_{\substack{x\notin\Psi_S^e\\ y\in\Psi_x}}\lambda_{xy}^t(\tau_{xy}^{RP}-\tau_{xy}^{SW})q_i^{xy,t}+\sum_{\substack{x\in\Psi_S^e\\ y\in\Psi_x}}n_i^{xy,t}\quad\forall i\in\Psi_N \tag{48}$$

$$\begin{cases}n_i^{xy,t}\ge u_{xy}^t-(1-p_i^{xy,t})M\\ n_i^{xy,t}\ge -p_i^{xy,t}M\\ n_i^{xy,t}\le u_{xy}^t+(1-p_i^{xy,t})M\\ n_i^{xy,t}\le p_i^{xy,t}M\end{cases}\quad x\in\Psi_S^e, y\in\Psi_x \tag{49}$$

III. Parallel Solution Process with Acceleration Method

This section introduces a parallelizable augmented Lagrangian algorithm [37], which is applicable for the split-variable reformulation of mixed-integer optimization problems, and is adopted to solve the coordination planning problem of the backbone grid and sub-areas. Independent planning of the backbone grid and sub-areas is achieved by solving the sub-problems in parallel. The global coordination is achieved by the iteration between the coordination layer and sub-problems.

A. Decomposable RcDNP Model

The algorithm presented in [37] is adapted to solve problems with the following form:

$$\min_{\boldsymbol{x}_i,\boldsymbol{z}_i,\forall i}\left\{\sum_{i=1}^{n}f_i(\boldsymbol{x}_i):\boldsymbol{Q}_i\boldsymbol{x}_i=\boldsymbol{z}_i,\boldsymbol{x}_i\in X_i,\forall i,\ (\boldsymbol{z}_1^{\mathrm{T}},\boldsymbol{z}_2^{\mathrm{T}},..,\boldsymbol{z}_n^{\mathrm{T}})^{\mathrm{T}}\in Z\right\} \tag{50}$$

where f_i is the objective function; $\boldsymbol{Q}_i$ is a matrix; and Z is the set of coordination variables. The model presented in the previous reference is a centralized model, which needs to be reorganized to adapt to the decomposition.

Combining the backbone grid and sub-areas, we can obtain the decomposed RcDNP model of the entire system:

$$\begin{cases}\min\ f(\boldsymbol{x}_b,\boldsymbol{x}_s)=f_b(\boldsymbol{x}_b)+\sum_{n=1}^{n_{sub}}f_{s,n}(\boldsymbol{x}_{s,n})\\ \text{s.t. (10)-(47) for backbone grid}\\ \qquad\text{(10)-(33), (36)-(44), (46)-(49) for sub-areas}\\ \qquad\text{(1)-(6)}\end{cases} \tag{51}$$

With the substitution of variables in (49), constraint (6) can be written as:

$$u_{i''j''}^t=CID_{i'}^{e,t}\quad i'\in\Psi_D^e, i''\in\Psi_S^e, j''\in\Psi_{i''} \tag{52}$$

To further organize the model into a form suitable for the parallelizable augmented Lagrangian algorithm, the decomposable RcDNP model can be written as the compact matrix form:

$$\begin{cases}\min f(\boldsymbol{x}_b,\boldsymbol{x}_s)=f_b(\boldsymbol{x}_b)+\sum_{n=1}^{n_{sub}}f_{s,n}(\boldsymbol{x}_{s,n})\\ \text{s.t. } \boldsymbol{x}_b\in X_b\\ \qquad\boldsymbol{x}_{s,n}\in X_{s,n}\\ \qquad Q_b\boldsymbol{x}_b=Q_{s,n}\boldsymbol{x}_{s,n}\\ \qquad n=1,2,...,n_{sub}\end{cases} \tag{53}$$

In order to make the structure of the model clearer, we further define $\boldsymbol{z}_b$ and $\boldsymbol{z}_{s,n}$ as:

$$Q_b\boldsymbol{x}_b=\boldsymbol{z}_b=[CIF_{i'}^{e,t},CID_{i'}^{e,t},P_{i'}^{d,t},Q_{i'}^{d,t},S_{i'j'}^{C,t},U_{i'}^{\mathrm{NO},t}]^{\mathrm{T}}\quad\forall i'\in\Psi_D^e, j'\in\Psi_{i'} \tag{54}$$

$$Q_{s,n}\boldsymbol{x}_{s,n}=\boldsymbol{z}_{s,n}=[\lambda_{i''j''}^t,u_{i''j''}^t,P_{i''j''}^{\mathrm{NO},t},Q_{i''j''}^{\mathrm{NO},t},S_{i''j''}^{C,t},U_{i''}^{ss,t}]^{\mathrm{T}}\quad i''\in\Psi_{S,n}^e, j''\in\Psi_{i''}, n=1,2,...,n_{sub} \tag{55}$$

Finally, the set Z is used to describe the coupling relationship between the coordination variables of different models, which is restricted by coordination constraints (1)-(5) and (52).

$$Z=\left\{[\boldsymbol{z}_b^{\mathrm{T}},\boldsymbol{z}_{s,1}^{\mathrm{T}},\ldots,\boldsymbol{z}_{s,n_{sub}}^{\mathrm{T}}]^{\mathrm{T}}\,\middle|\,(1)\text{-}(5),\,(52)\right\} \tag{56}$$

The coupling vectors of backbone grid $\boldsymbol{z}_b$ and sub-area $\boldsymbol{z}_{s,n}$ are confined to the regions constructed by coordination constraints. Thus, a decomposable RcDNP model is derived in the form of problem (50).

$$\begin{cases}\min\limits_{\boldsymbol{x},\boldsymbol{z}}\ f(\boldsymbol{x}_b,\boldsymbol{x}_s)=f_b(\boldsymbol{x}_b)+\sum\limits_{n=1}^{n_{sub}}f_{s,n}(\boldsymbol{x}_{s,n})\\ \text{s.t. } Q_b\boldsymbol{x}_b=\boldsymbol{z}_b\\ \quad \boldsymbol{x}_b\in X_b\\ \quad Q_{s,n}\boldsymbol{x}_{s,n}=\boldsymbol{z}_{s,n}\\ \quad \boldsymbol{x}_{s,n}\in X_{s,n}\\ \quad [\boldsymbol{z}_b^{\mathrm{T}},\boldsymbol{z}_{s,1}^{\mathrm{T}},\ldots,\boldsymbol{z}_{s,n_{sub}}^{\mathrm{T}}]^{\mathrm{T}}\in Z\end{cases} \tag{57}$$

Therefore, the parallelizable augmented Lagrangian algorithm can be adopted to solve problem (57). The detailed steps are described as follows.

1) *Step 1:* initialize. Define the augmented Lagrangian functions L_b and $L_{s,n}$ as:

$$L_b(\boldsymbol{x}_b,\boldsymbol{w}_b,\boldsymbol{z}_b)=f(\boldsymbol{x}_b)+\boldsymbol{w}_b^{\mathrm{T}}Q_b\boldsymbol{x}_b+\frac{\rho}{2}\left\|Q_b\boldsymbol{x}_b-\boldsymbol{z}_b\right\|^2 \tag{58}$$

$$L_{s,n}(\boldsymbol{x}_{s,n},\boldsymbol{w}_{s,n},\boldsymbol{z}_{s,n})=f(\boldsymbol{x}_{s,n})+\boldsymbol{w}_{s,n}^{\mathrm{T}}Q_{s,n}\boldsymbol{x}_{s,n}+\frac{\rho}{2}\left\|Q_{s,n}\boldsymbol{x}_{s,n}-\boldsymbol{z}_{s,n}\right\|^2 \tag{59}$$

Initialize parameters $\underline{\phi_b}=\underline{\phi_{s,n}}=-\infty$, $\rho>0$, $\varepsilon>0$, $k=0$, $T=0$, $\gamma\in(0,1)$, where $\underline{\phi_b}$ and $\underline{\phi_{s,n}}$ are dual functions in the planning problem of the backbone grid and the n^{th} sub-area, respectively; ε is the criterion to stop iteration; and γ is the parameter of the serious step condition.

2) *Step 2*: solve initial value of the sub-problem. Solve the problem of the backbone grid:

$$\begin{cases}(\text{P1})\ \min f_b(\boldsymbol{x}_b)=\sum\limits_{t=1}^{T}[\delta_t^I c_{t,b}^I+\delta_t^O(c_{t,b}^M+\omega\cdot EENS_b^t)]\\ \text{s.t. } \underline{P_{i'}^d}\le P_{i'}^{d,t}\le\overline{P_{i'}^d}\quad i'\in\Psi_D^e\\ \quad \underline{Q_{i'}^d}\le Q_{i'}^{d,t}\le\overline{Q_{i'}^d}\quad i'\in\Psi_D^e\\ \quad \underline{CIF_{i'}^e}\le CIF_{i'}^{e,t}\le\overline{CIF_{i'}^e}\quad i'\in\Psi_D^e\\ \quad \underline{CID_{i'}^e}\le CID_{i'}^{e,t}\le\overline{CID_{i'}^e}\quad i'\in\Psi_D^e\\ \quad (10)\text{-}(47)\end{cases} \tag{60}$$

Solve the planning model of each sub-area:

$$\begin{cases}(\text{P2})\ \min f_{s,n}(\boldsymbol{x}_{s,n})=\sum\limits_{t=1}^{T}[\delta_t^I c_{t,s,n}^I+\delta_t^O(c_{t,s,n}^M+\omega\cdot EENS_{s,n}^t)]\\ \text{s.t. } \underline{P_{i''j''}^{\mathrm{NO}}}\le P_{i''j''}^{\mathrm{NO},t}\le\overline{P_{i''j''}^{\mathrm{NO}}}\quad i''\in\Psi_{S,n}^e, j''\in\Psi_{i''}\\ \quad \underline{Q_{i''j''}^{\mathrm{NO}}}\le Q_{i''j''}^{\mathrm{NO},t}\le\overline{Q_{i''j''}^{\mathrm{NO}}}\quad i''\in\Psi_{S,n}^e, j''\in\Psi_{i''}\\ \quad \underline{\lambda_{i''j''}}\le\lambda_{i''j''}^t\le\overline{\lambda_{i''j''}}\quad i''\in\Psi_{S,n}^e, j''\in\Psi_{i''}\\ \quad \underline{u_{i''j''}}\le u_{i''j''}^t\le\overline{u_{i''j''}}\quad i''\in\Psi_{S,n}^e, j''\in\Psi_{i''}\\ \quad (10)\text{-}(33),\,(36)\text{-}(44),\,(46)\text{-}(49)\end{cases} \tag{61}$$

Construct the subset of the convex hull of the feasible regions $\boldsymbol{D}_b=\{\boldsymbol{x}_b^0\}$ and $\boldsymbol{D}_{s,n}=\{\boldsymbol{x}_{s,n}^0\}$ using the linear combination of above solution, where $\boldsymbol{x}_b^0$ is the solution of the backbone grid planning problem, and $\boldsymbol{x}_{s,n}^0$ is the solution of the n^{th} sub-area planning problem.

The coordination layer calculates coordination variables by solving the following optimization problem.

(P3) $\boldsymbol{z}^0=$

$$\arg\min_{\boldsymbol{z}_b,\boldsymbol{z}_{s,n}}\left\{\left\|Q_b\boldsymbol{x}_b^0-\boldsymbol{z}_b\right\|^2+\sum_{n=1}^{n_{sub}}\left\|Q_{s,n}\boldsymbol{x}_{s,n}^0-\boldsymbol{z}_{s,n}\right\|^2:\boldsymbol{z}_b,\boldsymbol{z}_{s,n}\in Z\right\} \tag{62}$$

where $\boldsymbol{z}^0=\{\boldsymbol{z}_b^0,\boldsymbol{z}_{s,1}^0,\ldots,\boldsymbol{z}_{s,n_{sub}}^0\}$ is the set of coordination variables for the backbone grid and all sub-area planning problems.

3) *Step 3*: update $k=k+1$, $T=1$.

4) *Step 4*: execute Gauss-Seidel iteration. Update variables: $\boldsymbol{x}_b^k=\boldsymbol{x}_b^{k-1}$, $\boldsymbol{x}_{s,n}^k=\boldsymbol{x}_{s,n}^{k-1}$, $\boldsymbol{z}^k=\boldsymbol{z}^{k-1}$, $\boldsymbol{w}_b^k=\boldsymbol{w}_b^{k-1}$, $\boldsymbol{w}_{s,n}^k=\boldsymbol{w}_{s,n}^{k-1}$, $\underline{\phi}^k=\underline{\phi}^{k-1}$, where $\underline{\phi}^k$ is the value of dual function in the k^{th} iteration.

Solve the optimization model for the backbone grid:

$$(\text{P4})\ \boldsymbol{x}_b^k=\arg\min_{\boldsymbol{x}_b}\{\{L_b(\boldsymbol{x}_b,\boldsymbol{w}_b^k,\boldsymbol{z}_b^k):\boldsymbol{x}_b\in\boldsymbol{D}_b\} \tag{63}$$

Solve the optimization model of each sub-area:

$$(\text{P5})\ \boldsymbol{x}_{s,n}^k=\arg\min_{\boldsymbol{x}_{s,n}}\{L_{s,n}(\boldsymbol{x}_{s,n},\boldsymbol{w}_{s,n}^k,\boldsymbol{z}_{s,n}^k):\boldsymbol{x}_{s,n}\in\boldsymbol{D}_{s,n}\} \tag{64}$$

Solve the model (P3) to update the coordination variables:

$$\boldsymbol{z}^k=\arg\min_{\boldsymbol{z}_b,\boldsymbol{z}_{s,n}}\left\{\left\|Q_b\boldsymbol{x}_b^k-\boldsymbol{z}_b\right\|^2+\sum_{n=1}^{n_{sub}}\left\|Q_{s,n}\boldsymbol{x}_{s,n}^k-\boldsymbol{z}_{s,n}\right\|^2:\boldsymbol{z}_b,\boldsymbol{z}_{s,n}\in Z\right\}.$$

5) *Step 5*: if $T\le T_{\max}$, $T=T+1$, return to *Step 4*. Otherwise, perform the following steps: $\tilde{\phi}_b=\underline{\phi_b}(\boldsymbol{w}_b^k+\rho(Q_b\boldsymbol{x}_b^k-\boldsymbol{z}_b^k))$, $\tilde{\phi}_{s,n}=\underline{\phi_{s,n}}(\boldsymbol{w}_{s,n}^k+\rho(Q_{s,n}\boldsymbol{x}_{s,n}^k-\boldsymbol{z}_{s,n}^k))$, where $\underline{\phi_b}(\boldsymbol{w}_b)$ and $\underline{\phi_{s,n}}(\boldsymbol{w}_{s,n})$ are defined as the dual functions of the original problems:

$$\underline{\phi_b}(\boldsymbol{w}_b)=\min_{\boldsymbol{x}_b}\{f_b(\boldsymbol{x}_b)+\boldsymbol{w}_b^{\mathrm{T}}Q_b\boldsymbol{x}_b:\boldsymbol{x}_b\in X_b\} \tag{65}$$

$$\underline{\phi_{s,n}}(\boldsymbol{w}_{s,n})=\min_{\boldsymbol{x}_{s,n}}\{f_{s,n}(\boldsymbol{x}_{s,n})+\boldsymbol{w}_{s,n}^{\mathrm{T}}Q_{s,n}\boldsymbol{x}_{s,n}:\boldsymbol{x}_{s,n}\in X_{s,n}\} \tag{66}$$

where the variables with "~" and "^" are temporary variables.

Solve the optimization model of the backbone grid:

$$(\text{P6})\ \hat{\boldsymbol{x}}_b=\arg\min_{\boldsymbol{x}_b}\{\underline{\phi_b}(\boldsymbol{w}_b^k+\rho(Q_b\boldsymbol{x}_b^k-\boldsymbol{z}_b^k))\} \tag{67}$$

Solve the optimization model of each sub-area:

$$(\text{P7})\ \hat{\boldsymbol{x}}_{s,n}=\arg\min_{\boldsymbol{x}_{s,n}}\{\underline{\phi_{s,n}}(\boldsymbol{w}_{s,n}^k+\rho(Q_{s,n}\boldsymbol{x}_{s,n}^k-\boldsymbol{z}_{s,n}^k))\} \tag{68}$$

Add the vertex to the subset of the convex hull of the feasible region: $\boldsymbol{D}_b=conv(\boldsymbol{D}_b\cup\{\hat{\boldsymbol{x}}_b\})$, $\boldsymbol{D}_{s,n}=conv(\boldsymbol{D}_{s,n}\cup\{\hat{\boldsymbol{x}}_{s,n}\})$, $\varepsilon_b^k=\hat{\phi}_b(\boldsymbol{w}_b^k,\boldsymbol{x}_b^k,\boldsymbol{z}_b^k)-\underline{\phi_b^k}$, $\varepsilon_{s,n}^k=\hat{\phi}_{s,n}(\boldsymbol{w}_{s,n}^k,\boldsymbol{x}_{s,n}^k,\boldsymbol{z}_{s,n}^k)-\underline{\phi_{s,n}^k}$, $\Delta\phi_b^k=\tilde{\phi}_b-\underline{\phi_b^k}$, $\Delta\phi_{s,n}^k=\tilde{\phi}_{s,n}-\underline{\phi_{s,n}^k}$, where $\hat{\phi}_b(\boldsymbol{w}_b,\boldsymbol{x}_b,\boldsymbol{z}_b)$ and $\hat{\phi}_{s,n}(\boldsymbol{w}_{s,n},\boldsymbol{x}_{s,n},\boldsymbol{z}_{s,n})$ are the cutting plane functions used to approximate the dual function (65) and (66), which are defined as:

$$\hat{\phi}_b(\boldsymbol{w}_b,\boldsymbol{x}_b,\boldsymbol{z}_b)=L_b(\boldsymbol{x}_b,\boldsymbol{w}_b,\boldsymbol{z}_b)+\frac{\rho}{2}\left\|Q_b\boldsymbol{x}_b-\boldsymbol{z}_b\right\|^2 \tag{69}$$

$$\hat{\phi}_{s,n}(\boldsymbol{w}_{s,n},\boldsymbol{x}_{s,n},\boldsymbol{z}_{s,n})=L_{s,n}(\boldsymbol{x}_{s,n},\boldsymbol{w}_{s,n},\boldsymbol{z}_{s,n})+\frac{\rho}{2}\left\|Q_{s,n}\boldsymbol{x}_{s,n}-\boldsymbol{z}_{s,n}\right\|^2 \tag{70}$$

The algorithm converges if the gaps ε_b^k and $\varepsilon_{s,n}^k$ are small enough.

6) *Step 6*: check the convergence criterion. If $\varepsilon_b^k+\sum\limits_{n=1}^{n_{sub}}\varepsilon_{s,n}^k\le\varepsilon$,

the algorithm converges. Otherwise, perform the following steps.

Calculate $\eta^k=\Delta\phi_b^k/\varepsilon_b^k+\sum\limits_{n=1}^{n_{sub}}\Delta\phi_{s,n}^k/\varepsilon_{s,n}^k$. If $\eta^k\ge\gamma$, the Nesterov acceleration method with restart is adopted to update $\boldsymbol{w}_b^k$ and $\boldsymbol{w}_{s,n}^k$ [38].

7) *Step 7*: update ρ: $\dfrac{1}{\rho}=\min\left\{\max\left\{\dfrac{2}{\rho}(1-\eta^k),\dfrac{1}{10\rho},\dfrac{1}{\rho_{\max}}\right\},\dfrac{10}{\rho},\dfrac{1}{\rho_{\min}}\right\}$. If $k>k_{\max}$, the algorithm stops. Otherwise, return to *Step 3*.

The flowchart depicting the solution process is presented in Fig. 3.

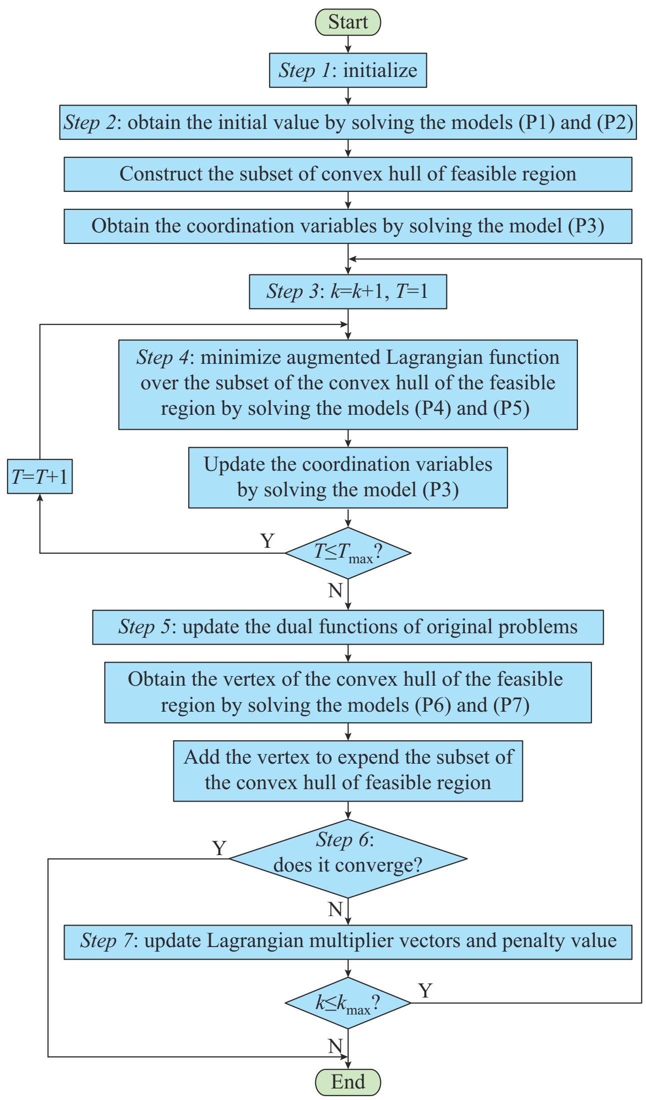

Fig. 3. Flowchart depicting solution process.

B. Optimality and Convergence

In Section III-A, the RcDNP model is reformed to adapt to the algorithm in [37]. Since the objective function $f(\boldsymbol{x})$ is linear, the solution of (57) can be obtained by optimizing on the convex hull $conv(X)$ of the original domain, i.e.,

$$\min_{\boldsymbol{x},\boldsymbol{z}}\ \{f(\boldsymbol{x}):\boldsymbol{Qx}=\boldsymbol{z},\boldsymbol{x}\in conv(X),\boldsymbol{z}\in Z\} \tag{71}$$

In [37], based on the conclusion of Proposition 3 and Lemma 1, Proposition 4 proves that the sequence $\{(\boldsymbol{x}^k,\boldsymbol{z}^k)\}$ generated by *Step 4* in the main loop has limit points, which is optimal for (71). Thus, it is also the optimal solution of the original problem (57).

In order to analyze the rate of convergence, the dual function of the convex relaxation (71) is introduced as:

$$\phi^C(\boldsymbol{w})=\min_{\boldsymbol{x},\boldsymbol{z}}\ \{f(\boldsymbol{x})+\boldsymbol{w}^{\mathrm{T}}(\boldsymbol{Qx}-\boldsymbol{z}),\boldsymbol{x}\in conv(X),\boldsymbol{z}\in Z\} \tag{72}$$

Assume that the original problem has an optimal dual solution $\boldsymbol{w}^*$. According to Proposition 2 in [37], the sum of the gap between $\phi^C(\boldsymbol{w}^*)$ and $\underline{\phi}^k$ in all iterations is limited. For the case that parameter ρ is fixed, the following conclusion holds:

$$\sum_{k=1}^{N}(\phi^C(\boldsymbol{w}^*)-\underline{\phi}^k)<\infty \tag{73}$$

Considering that $\underline{\phi}^k$ is non-decreasing, we have:

$$\phi^C(\boldsymbol{w}^*)-\underline{\phi}^k=o(1/k) \tag{74}$$

For the case where parameters ρ and γ both vary but satisfy $\rho_k(1/\gamma_k-1)=c$, the rate of convergence can be quadratic. It is worth noting that the actual convergence rate may not reach the theoretical level since the serious step condition may not be guaranteed in each iteration.

After adopting Nesterov acceleration method with restart, the parallelizable augmented Lagrangian algorithm will perform one of the following three operations when updating the dual variable: ① a "restart"; ② a "nonaccelerated" step immediately after a "restart", in which the acceleration factor $\alpha_k=1$; ③ an "accelerated" step, in which $\alpha_k>1$. According to Theorem 3 in [38], the residual c_k decreases by at least a factor of δ in an accelerated step. Therefore, after k iterations, we can obtain:

$$c_k\le c_0\delta^{\hat{k}} \tag{75}$$

where $\hat{k}$ is the number of acceleration steps performed.

If there are enough acceleration steps, we will have $c_k\to 0$. And after the last acceleration step, the dual variable updating will be equivalent to the original algorithm, for which the convergence is known. The numerical test in [38] proves the advantages of the restart. Research works on restarted variants of other acceleration methods also share similar results [39].

IV. Numerical Tests

The RcDNP model and proposed solution method is tested on the planning of backbone grid and different numbers of sub-areas. System data can be accessed from [40]. All numerical tests are carried out on a laptop computer with an Intel Core i7-10875H CPU and 16 GB RAM. The MILP model is solved by Gurobi (version 9.5.0).

A. Backbone Grid and Two Sub-areas

The backbone grid consists of eight nodes and each sub-area consists of 20 nodes. Branch and node parameters partly come from [25]. The topology of the test system can be found in [41].

The results and solution time of the proposed method are compared with the centralized method [25]. The extended planning results of the two methods for the backbone grid and two sub-areas are shown in Fig. 4. Reliability evaluation [5] is used to verify the results to ensure that the results meet the reliability requirements. The reliability indices, construction costs, and solution time of the two methods are listed in the Table I.

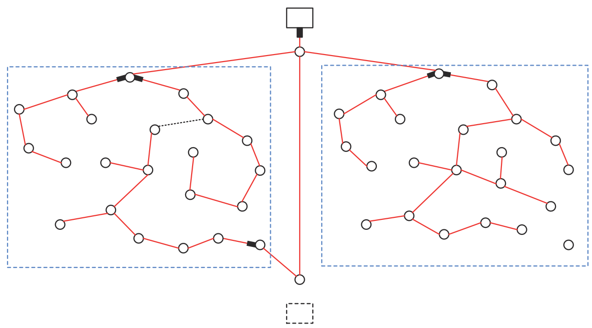

Fig. 4. Extended planning results of two methods for backbone grid and two sub-areas.

TABLE I
RELIABILITY INDICES, CONSTRUCTION COSTS, AND SOLUTION TIME OF TWO METHODS

Method	Required SAIDI (area 1)	Evaluated SAIDI (area 1)	Required SAIDI (area 2)	Evaluated SAIDI (area 2)	Total cost (k$)	Solution time (s)
Centralized	1.5	1.4997	2	1.978	1007	1335
Proposed	1.5	1.4997	2	1.978	1007	929

It can be observed that the constructed branches and the operation mode planned by the proposed method are the same as those planned by the centralized method. However, due to the parallel solution architecture, the proposed method solves the problem faster than the centralized method.

B. Backbone Grid and Three Sub-areas

Another numerical test is conducted on a larger-scale case with a backbone grid and three sub-areas. The detailed setting of this case can be found in [41].

The planning results of the centralized planning method and the proposed method for the backbone grid and three sub-areas are shown in Fig. 5. We have compared the proposed method with traditional centralized method and parallel solving method based on genetic algorithm. The construction costs and solution time of different methods are listed in Table II.

The effect of the acceleration method is shown in Fig. 6. It can be observed that the convergence speed is significantly improved by introducing the acceleration method. The method with acceleration method converges to the optimal value (1243 k$) at the 30[th] iteration, while the method without acceleration method only reaches 1255 k$ in the same iteration steps.

The effect of the proposed method on multi-stage planning problems and the model considering the uncertainties of load and distributed generation are shown in [41].

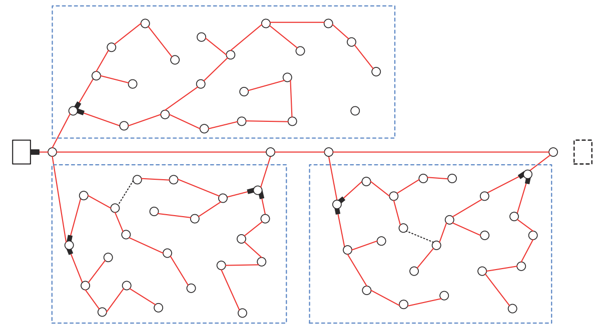

Fig. 5. Extended planning results of two methods for backbone grid and three sub-areas.

TABLE II
CONSTRUCTION COSTS AND SOLUTION TIME OF PLANNING RESULTS OF DIFFERENT METHODS

Method	Total cost (k$)	Solution time (s)
Centralized method	1243	6980
Proposed method	1243	1935
Parallel solving method based on genetic algorithm	1355	85758

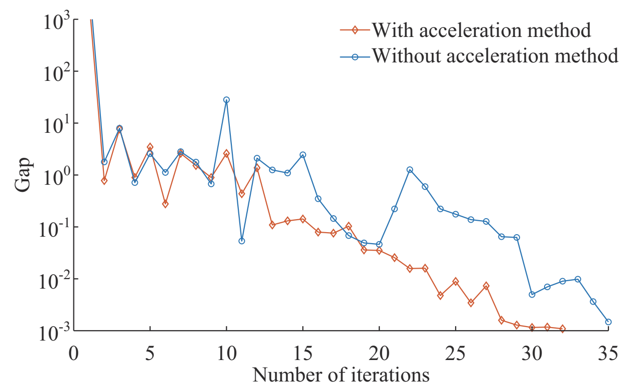

Fig. 6. Effects of acceleration method.

C. Backbone Grid and Six Sub-areas

We further expand the scale of the case to a 139-node DN containing a backbone grid and six sub-areas. As the scale of the centralized model is too large, it cannot be solved in an acceptable time. There are only the results of the parallel computing method shown in Fig. 7. The results of the proposed method with acceleration for the 139-node DN are listed in Table III. When the centralized method is adopted, the gap of the solution is still 22.02% after seven days, and the total cost of the planning scheme is 51333 k$.

D. 1495-node Test System

To further verify the scalability of the proposed method, a 1495-node test system consisting of a backbone grid and 10 sub-areas is used to test the proposed method. The backbone grid is a modified 85-node DN and the sub-area is a modified 141-node DN, the information of which can be found in

MATPOWER [42]. The results of the proposed method with the acceleration are shown in Table IV, while the centralized method still cannot obtain the solution after seven days.

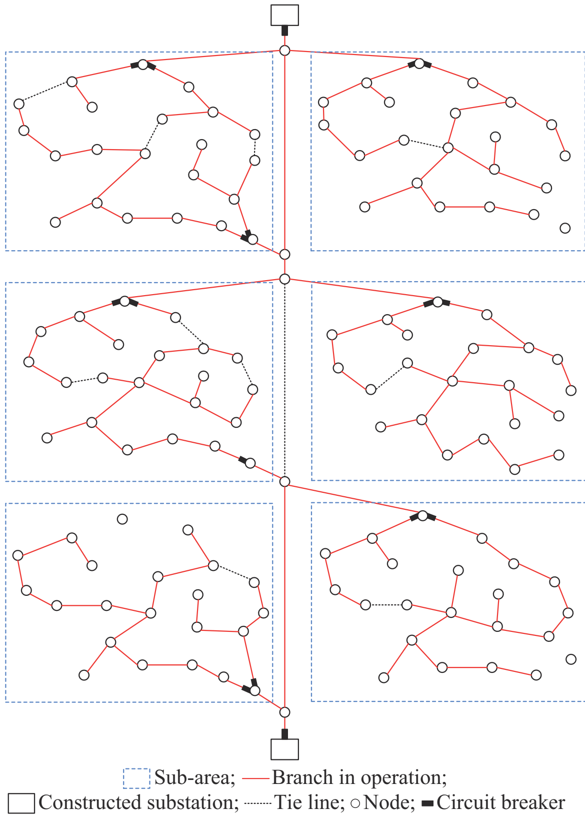

Fig. 7. Extended planning results of proposed method for backbone grid and six sub-areas.

TABLE III
RESULTS OF PROPOSED METHOD WITH ACCELERATION FOR 139-NODE DN

Total cost (k$)	Required SAIDI	SAIDI	Solution time (s)
40429	1.9	1.8481	5358
	2.6	2.5951	
	2.2	1.9973	
	2.8	2.7961	
	2.4	2.3895	
	2.9	2.7823	

TABLE IV
RESULTS OF PROPOSED METHOD WITH ACCELERATION FOR 1495-NODE TEST SYSTEM

Total cost (k$)	Required SAIDI	SAIDI	Solution time (s)
71411	1.5	1.4977	98036
	1.4	1.3494	
	1.7	1.6998	
	1.6	1.5794	
	1.8	1.7983	
	1.5	1.4850	
	1.4	1.3749	
	1.7	1.6699	
	2.0	1.9158	
	1.9	1.8987	

E. Analysis of Solution Efficiency

For MILP problems, the number of binary variables can roughly reflect the size of the problem. The search space of the MILP problem rapidly expands with the increase of binary variables.

Table V illustrates the comparison of the number of binary variables between centralized method and the proposed method for the different systems.

TABLE V
NUMBER OF BINARY VARIABLES BETWEEN CENTRALIZED METHOD AND PROPOSED METHOD

System	Number of binary variables	
	Centralized method	Proposed method
48-node	12620	4736
72-node	24398	6800
139-node	82820	12992
1495-node	7130296	56236

As the system scale increases, the number of binary variables in the centralized method will explosively grow, leading to a significant expansion of the search space. To provide a more intuitive illustration, a comparison graph for the number of binary variables and solution time of the two methods at different numbers of sub-areas is shown in Fig. 8.

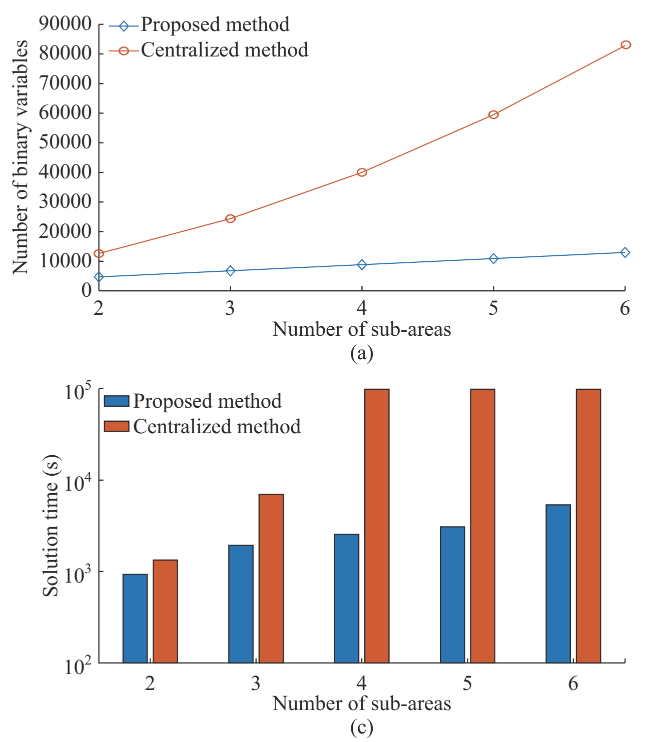

Fig. 8. Comparison of centralized method and proposed method in terms of number of binary variables and solution time. (a) Number of binary variables. (b) Solution time.

It can be observed that as the size of the DN increases, the number of binary variables in the centralized method rises rapidly, while the number of binary variables in the parallel computing method increases almost linearly with the problem size. The rapid expansion of the model size not only makes the modeling more challenging, but also makes it more difficult to obtain an optimal or even feasible solution within an acceptable time. From the comparison graph of solution time, it can be observed that when the case increases to four sub-areas, the running time of centralized method has exceeded one day while the proposed method converges within the acceptable time in all the cases. The proposed method demonstrates a significant advantage in terms of efficiency.

V. Conclusion

We propose a parallel computing based solution method for solving the RcDNP problem. A decomposition planning model containing the backbone grid and sub-areas is presented, in which the integer variables increase linearly with the size of networks, while those in the original model increase quadratically. A parallelizable augmented Lagrangian algorithm incorporating Nesterov acceleration method with restart is adopted to solve the RcDNP model. Numerical tests on different systems demonstrate that the proposed method has significant advantages in terms of solution efficiency on the premise of ensuring optimality. The proposed method enables the RcDNP model with the potentiality of real-world application.

References

[1] C. Gandioli, M.-C. Alvarez-Hérault, P. Tixador *et al.*, "Innovative distribution networks planning integrating superconducting fault current limiters," *IEEE Transactions on Applied Superconductivity*, vol. 23, no. 3, pp. 5603904-5603904, Jun. 2013.

[2] D. S. Kumar, D. Srinivasan, A. Sharma *et al.*, "Adaptive directional overcurrent relaying scheme for meshed distribution networks," *IET Generation, Transmission & Distribution*, vol. 12, no. 13, pp. 3212-3220, Jul. 2018.

[3] M. Gholami, J. Moshtagh, and N. Ghadernejad, "Service restoration in distribution networks using combination of two heuristic methods considering load shedding," *Journal of Modern Power Systems and Clean Energy*, vol. 3, no. 4, pp. 556-564, Dec. 2015.

[4] F. R. Islam, K. Prakash, K. A. Mamun *et al.*, "Aromatic network: a novel structure for power distribution system," *IEEE Access*, vol. 5, pp. 25236-25257, Oct. 2017.

[5] Z. Li, W. Wu, B. Zhang *et al.*, "Analytical reliability assessment method for complex distribution networks considering post-fault network reconfiguration," *IEEE Transactions on Power Systems*, vol. 35, no. 2, pp. 1457-1467, Mar. 2020.

[6] H. L. Willis, *Power Distribution Planning Reference Book*, 2nd ed. New York: Marcel Dekker, 2004.

[7] *IEEE Guide for Electric Power Distribution Reliability Indices*, IEEE Standard 1366-2003, May 2004.

[8] Y. Tang, "Power distribution system planning with reliability modeling and optimization," *IEEE Transactions on Power Systems*, vol. 11, no. 1, pp. 181-189, Feb. 1996.

[9] R. E. Brown, S. Gupta, R. D. Christie *et al.*, "Automated primary distribution system design: reliability and cost optimization," *IEEE Transactions on Power Delivery*, vol. 12, no. 2, pp. 1017-1022, Apr. 1997.

[10] A. A. Chowdhury and D. O. Koval, *Power Distribution System Reliability: Practical Methods and Applications*. Hoboken: Wiley, 2009.

[11] R. C. Lotero and J. Contreras, "Distribution system planning with reliability," *IEEE Transactions on Power Delivery*, vol. 26, no. 4, pp. 2552-2562, Oct. 2011.

[12] I. Ziari, G. Ledwich, A. Ghosh *et al.*, "Optimal distribution network reinforcement considering load growth, line loss, and reliability," *IEEE Transactions on Power Systems*, vol. 28, no. 2, pp. 587-597, May 2013.

[13] S. M. Mazhari, H. Monsef, and R. Romero, "A multi-objective distribution system expansion planning incorporating customer choices on reliability," *IEEE Transactions on Power Systems*, vol. 31, no. 2, pp. 1330-1340, Mar. 2016.

[14] I. Hernando-Gil, I.-S. Ilie, and S. Z. Djokic, "Reliability planning of active distribution systems incorporating regulator requirements and network-reliability equivalents," *IET Generation, Transmission & Distribution*, vol. 10, no. 1, pp. 93-106, Jan. 2016.

[15] N. N. Mansor and V. Levi, "Integrated planning of distribution networks considering utility planning concepts," *IEEE Transactions on Power Systems*, vol. 32, no. 6, pp. 4656-4672, Nov. 2017.

[16] I. J. Ramirez-Rosado and J. A. Dominguez-Navarro, "Possibilistic model based on fuzzy sets for the multiobjective optimal planning of electric power distribution networks," *IEEE Transactions on Power Systems*, vol. 19, no. 4, pp. 1801-1810, Nov. 2004.

[17] N. N. Mansor and V. Levi, "Operational planning of distribution networks based on utility planning concepts," *IEEE Transactions on Power Systems*, vol. 34, no. 3, pp. 2114-2127, May 2019.

[18] C. Wang, T. Zhang, F. Luo *et al.*, "Fault incidence matrix based reliability evaluation method for complex distribution system," *IEEE Transactions on Power Systems*, vol. 33, no. 6, pp. 6736-6745, Nov. 2018.

[19] T. Zhang, C. Wang, F. Luo *et al.*, "Optimal design of the sectional switch and tie line for the distribution network based on the fault incidence matrix," *IEEE Transactions on Power Systems*, vol. 34, no. 6, pp. 4869-4879, Nov. 2019.

[20] M. Jooshaki, A. Abbaspour, M. Fotuhi-Firuzabad *et al.*, "MILP model of electricity distribution system expansion planning considering incentive reliability regulations," *IEEE Transactions on Power Systems*, vol. 34, no. 6, pp. 4300-4316, Nov. 2019.

[21] R. H. Fletcher and K. Strunz, "Optimal distribution system horizon planning – part I: formulation," *IEEE Transactions on Power Systems*, vol. 22, no. 2, pp. 791-799, May 2007.

[22] R. H. Fletcher and K. Strunz, "Optimal distribution system horizon planning – part II: application," *IEEE Transactions on Power Systems*, vol. 22, no. 2, pp. 862-870, May 2007.

[23] G. Muñoz-Delgado, J. Contreras, and J. M. Arroyo, "Distribution network expansion planning with an explicit formulation for reliability assessment," *IEEE Transactions on Power Systems*, vol. 33, no. 3, pp. 2583-2596, May 2018.

[24] A. Bosisio, A. Berizzi, D. Lupis *et al.*, "A tabu-search-based algorithm for distribution network restoration to improve reliability and resiliency," *Journal of Modern Power Systems and Clean Energy*, vol. 11, no. 1, pp. 302-311, Jan. 2023.

[25] Z. Li, W. Wu, X. Tai *et al.*, "A reliability-constrained expansion planning model for mesh distribution networks," *IEEE Transactions on Power Systems*, vol. 36, no. 2, pp. 948-960, Mar. 2021.

[26] C. Lin and S. Lin, "Distributed optimal power flow with discrete control variables of large distributed power systems," *IEEE Transactions on Power Systems*, vol. 23, no. 3, pp. 1383-1392, Aug. 2008.

[27] Z. Tang, D. J. Hill, and T. Liu, "Fast distributed reactive power control for voltage regulation in distribution networks," *IEEE Transactions on Power Systems*, vol. 34, no. 1, pp. 802-805, Jan. 2019.

[28] Y. Wang, L. Wu, and S. Wang, "A fully-decentralized consensus-based ADMM approach for DC-OPF with demand response," *IEEE Transactions on Smart Grid*, vol. 8, no. 6, pp. 2637-2647, Nov. 2017.

[29] A. Mohammadi, M. Mehrtash, and A. Kargarian, "Diagonal quadratic approximation for decentralized collaborative TSO + DSO optimal power flow," *IEEE Transactions on Smart Grid*, vol. 10, no. 3, pp. 2358-2370, May 2019.

[30] J. C. Moreira, E. Miguez, C. Vilacha *et al.*, "Large-scale network layout optimization for radial distribution networks by parallel computing," *IEEE Transactions on Power Delivery*, vol. 26, no. 3, pp. 1946-1951, Jul. 2011.

[31] J. C. Moreira, E. Miguez, C. Vilacha *et al.*, "Large-scale network layout optimization for radial distribution networks by parallel computing: implementation and numerical results," *IEEE Transactions on Power Delivery*, vol. 27, no. 3, pp. 1468-1476, Jul. 2012.

[32] J. R. E. Fletcher, T. Fernando, H. H.-C. Iu *et al.*, "Spatial optimization for the planning of sparse power distribution networks," *IEEE Transactions on Power Systems*, vol. 33, no. 6, pp. 6686-6695, Nov. 2018.

[33] Ž. N. Popović, V. D. Kerleta, and D. S. Popović, "Hybrid simulated annealing and mixed integer linear programming algorithm for optimal planning of radial distribution networks with distributed generation," *Electric Power Systems Research*, vol. 108, pp. 211-222, Mar. 2014,

[34] S. M. Mazhari, H. Monsef, and R. Romero, "A hybrid heuristic and evolutionary algorithm for distribution substation planning," *IEEE Systems Journal*, vol. 9, no. 4, pp. 1396-1408, Dec. 2015.

[35] S. Heidari and M. Fotuhi-Firuzabad, "Integrated planning for distribution automation and network capacity expansion," *IEEE Transactions*

on Smart Grid, vol. 10, no. 4, pp. 4279-4288, Jul. 2019.

[36] A. Navarro and H. Rudnick, "Large-scale distribution planning – part II: macro-optimization with Voronoi's diagram and tabu search," *IEEE Transactions on Power Systems*, vol. 24, no. 2, pp. 752-758, May 2009.

[37] B. Dandurand, N. Boland, J. Christiansen *et al.*, "A parallelizable augmented lagrangian method applied to large-scale non-convex-constrained optimization problems," *Mathematical Programming*, vol. 175, no. 1-2, pp. 503-536, May 2019.

[38] T. Goldstein, B. O'Donoghue, S. Setzer *et al.*, "Fast alternating direction optimization methods," *SIAM Journal on Imaging Sciences*, vol. 7, no. 3, pp. 1588-1623, Jan. 2014.

[39] B. O'Donoghue and E. Candès, "Adaptive restart for accelerated gradient Schemes," *Foundations of Computational Mathematics*, vol. 15, no. 3, pp. 715-732, Jun. 2015.

[40] Y. Sun, W. Wu, Y. Lin *et al.* (2023, Oct.). Data for case studies. [Online]. Available: https://www.jianguoyun.com/p/DXWXhKoQ5ZijCRjX2p4FIAA

[41] Y. Sun, W. Wu, Y. Lin *et al.* (2023, Oct.). Supplemental file for parallel computing based solution for reliability-constrained distribution network planning. [Online]. Available: https://www. jianguoyun. com/p/DVEJNn0Q5ZijCRif4p4FIAA

[42] R. D. Zimmerman and C. E. Murillo-Sanchez. (2020, Dec.). MATPOWER (Version 7.1). [Online]. Available: https://matpower.org

Yaqi Sun received the B.S. degree in electrical engineering from Xi'an Jiaotong University, Xi'an, China, in 2020. He is currently pursuing the Ph.D. degree in electrical engineering in Tsinghua University, Beijing, China. His research interests include distribution network reliability assessment and distribution network planning with reliability constraints.

Wenchuan Wu received the B.S., M.S., and Ph.D. degrees from the Department of Electrical Engineering, Tsinghua University, Beijing, China. He is currently a Professor with Tsinghua University, and the Deputy Director of the State Key Laboratory of Power Systems. His research interests include energy management system, active distribution system operation and control, and machine learning and its application in energy systems.

Yi Lin received the B.S. and M.S. degrees in electrical engineering from Tsinghua University, Beijing, China, in 2009 and 2012. His research interests include power network planning, optimization of power system, and integrated energy system.

Hai Huang is an Engineer with State Grid Fujian Electric Power Co. Ltd., Fuzhou, China. His research interests include power system planning, design, and development.

Hao Chen is an Engineer with State Grid Fujian Electric Power Co. Ltd., Fuzhou, China. His research interests include distribution network planning, electromagnetic compatibility, and power quality.